J Mater Sci (2020) 55:15117–15129

Ceramics

Cold sintering zinc oxide with a crystalline zinc acetate dihydrate mass transport phase

Richard D. Floyd Jr.[1], Sarah Lowum[1,*], and Jon-Paul Maria[1]

[1] *Department of Materials Science and Engineering, The Pennsylvania State University, 215 Steidle Building, University Park, PA 16802, USA*

Received: 17 April 2020
Accepted: 1 August 2020
Published online: 7 August 2020

ABSTRACT

Cold sintering of ZnO using crystalline zinc acetate dihydrate in the absence of added water is examined. Prior studies use an aqueous solvent, usually containing a weak acid, base, or organic salt, as the mass transport phase during cold sintering. This paper shows equivalent densification of ZnO using solid, powdered acetate as compared to previously mentioned aqueous-based transport phases. It also presents the potential to add zinc acetate in higher quantities without increasing the amount of total added transport phase, as solubility limits in aqueous solvents define the maximum amount of zinc acetate that can be added for a given volume of liquid. Experiments were conducted using the previously reported sinterometer, allowing for in situ experimental monitoring to show densification trends of this new transport phase as a function of concentration, time, and temperature. The potentially dramatic impacts of varying humidity during powder preparation on final sample density will also be discussed.

Introduction

Recently, motivated by initial reports from Randall et al., the international ceramics community demonstrated the possibility for cold sintering, a method to densify ceramic powders using a secondary transport phase and moderate uniaxial pressures in a temperature range below several hundred degrees Centigrade [1]. The low thermal budget required by cold sintering provides an avenue to synthesize dense polycrystalline monoliths that are otherwise not possible to sinter due to volatility or high temperature degradation/decomposition [2]. This process has been applied to a variety of ceramic oxides, ceramic-ceramic composites, and polymer-ceramic composites with success [3].

With few exceptions [4, 5], aqueous solutions are the preferred and reported mass transport phases facilitating the process [3, 6–11]. For the case of ZnO, aqueous solutions of acetic acid (HOAc) or zinc acetate ($Zn(OAc)_2$) can densify particle compacts to near theoretical limits just above the boiling point of H_2O with no apparent secondary phase formation [12]. However, in materials such as $BaTiO_3$, aqueous transport phases promote amorphous glassy phases that require post-cold sintering heat treatments to

Address correspondence to E-mail: sml92@psu.edu

https://doi.org/10.1007/s10853-020-05100-9

eliminate [13, 14]. Potential avenues that prevent this amorphous phase tune the transport phase to chemically react with the parent oxide, such as the case of reactive phase cold sintering. However, this process still requires a heat treatment at 950 °C to complete the chemical reaction [15]. Aqueous solutions can also promote formation of unwanted hydroxide phases, requiring a non-aqueous transport phase. Dimethyl sulfoxide (DMSO) has been targeted as a potential avenue to densify MnO while avoiding $Mn(OH)_2$ formation [4].

Current models to describe the cold sintering process range from dissolution and precipitation to hydrothermal-like growth [2, 3]. These models are limited to specific cases requiring finite amounts of water (i.e., tens of volume percent) to facilitate densification [3]. Work done by Hong et al. and Li et al. investigated NaCl densification using additional water content under 10 vol.% [8, 16]. However, an understanding into the role of water that is either adsorbed to the surface of the powders or structurally bound to the transport phase is non-existent. The effects of relative humidity during powder preparation and storage are also inadequately studied.

This paper discusses a series of experiments where ZnO is cold-sintered with a $Zn(OAc)_2$ transport phase added as both a liquid, aqueous solution form and as a solid form by using crystalline $Zn(OAc)_2{\cdot}2H_2O$ without added water. In comparison with earlier reports [12], this study employs in situ capabilities to track the compaction profile of each experiment. This is done using an automated uniaxial press, referred to as the sinterometer, whose isothermal and isobaric design is uniquely suited for cold sintering experiments [17]. Comparisons between solid and liquid zinc acetate transport phases will be given in terms of both final sample density and compaction profiles. Further studies explore the effect of relative humidity on ZnO compaction profiles when $Zn(OAc)_2{\cdot}2H_2O$ is the sole transport phase.

Experimental procedures

ZnO (Alfa Aesar, 44263, 99.9%) was ball-milled in methanol for 48 h and subsequently dried in a rotary evaporator. For aqueous experiments, solutions of $Zn(OAc)_2{\cdot}2H_2O$ (Alfa Aesar, A12909, > 97%) were prepared in varying concentrations and added to the ZnO powder (typically ~ 1 g batches) in a 4 wt.% (~ 20 vol.%) fraction. For non-aqueous experiments, the same crystalline $Zn(OAc)_2{\cdot}2H_2O$ powder was milled into a fine powder using a SPEX mill and then added to the ZnO powder in equivalent mol.% concentrations as those of the aqueous solutions. Powders were thoroughly mixed in a SpeedMixer™ (Flacktek Inc., Model DAC150.1 FVZ) before either immediately pouring into a 1/2-inch stainless steel pellet die and pressed or transferred to a humidity-controlled environment as described below.

Saturated salt solutions were used to control relative humidity of the powder storage environment for non-aqueous experiments. Salt solutions were kept at room temperature (20 °C) in sealed plastic containers. SpeedMixed powders were equilibrated with each saturated salt solution for at least one day before pressing. Humidity cards (Traceable® Humidity-On-A-Card™) were used to ensure each container was equilibrated at the proper humidity according to Table 1 [18, 19].

Equilibrated powders were transferred to a pellet die for pressing. Most experiments were conducted in a custom-designed "turbo" die [17]. This die was fabricated from hardened 440C stainless steel with a ½″ internal diameter. The die was heated by eight 300 W cartridge heaters placed in holes drilled around the circumference of the die. The heaters were powered by a 220 V supply. Temperature was monitored by a 1/16″ probe thermocouple sitting 1/8″ away from the sample in the die. A low-profile thermocouple placed on the interior die wall confirmed that the reading from the probe thermocouple aligned with the internal die temperature. A Eurotherm 2048 temperature controller was used to maintain uniform ramp rates (~ 80 °C/min) and dwell temperatures. As noted later in the text, one set of early experiments was conducted in an older ½″ hardened 440C stainless steel pellet die heated by a

Table 1 Relative humidity of saturated salt solutions at 20 °C [18]

Material	Relative humidity at 20 °C (%)
Potassium acetate	23
Potassium carbonate	43
Magnesium nitrate	54
Sodium chloride	75
Potassium chloride	85

400 W band heater, which had slower ramp rates around 20 °C/min. Temperature of this die was monitored by a low-profile thermocouple stuck on the outside of the die underneath the band heater. Since the thermocouple was farther from the sample in this case, temperature calibrations were performed with a second thermocouple placed on the internal die wall to verify the actual sample temperature aligned with the temperature reading of the die. By the time the external temperature reading reached the 120 °C set-point, the internal temperature only lagged behind by ~ 5 °C and equilibrated within a couple minutes.

Once loaded in the pellet die, samples were pressed in an ambient laboratory environment using the sinterometer, a custom press introduced in a previous report [17]. The press is backed by an electric-hydraulic motor, maintaining constant pressure via a single-stage regulator. The resulting powder compaction is directly recorded with an extensometer mounted to the press cylinder. For all experiments, the desired pressure is first applied to the room-temperature pellet die, then the heat is turned on at time "0". Pressure remains constant during the temperature ramp and isothermal stages of cold sintering. Die temperature is recorded using a USB-thermocouple adapter.

Combined, the automated press and temperature-controlled pellet die allow for long-term experiments under controlled isobaric and isothermal conditions. Plots of compaction vs. time are presented in the form of "*sintegrams*", which account for thermal expansion resulting from the heating of the pellet die.

Density was measured geometrically and compared against the theoretical density of ZnO (5.61 g/cm^3) to calculate the relative density. Final cold-sintered samples were 12.7 mm in diameter (determined by the ½" pellet die) and high-density samples were ~ 1.4 mm thick, while low density samples were up to ~ 2.0 mm thick. X-ray diffraction (XRD—Panalytical Empyrean, Cu K-α radiation) was used to investigate sample crystallinity and phase purity. Starting powder was scanned in powder form, while cold-sintered samples were scanned in bulk form after surfaces were polished with sandpaper. Scanning electron microscopy (SEM—Zeiss Sigma VP-FESEM, 1 kV accelerating voltage) was used to analyze fracture surfaces. Trace quantities of secondary phase were investigated with thermogravimetric analysis (TGA—Netzsch Jupiter STA 445) in an oxygen environment at a heating rate of 15 °C/min.

Results and discussion

Densification using $Zn(OAc)_2$ solutions

ZnO pellets were densified with varying molarities of $Zn(OAc)_2$ aqueous solutions, ranging from 0.2 M to 1.2 M. The total amount of added transport phase solution was held constant at 4 wt.% (~ 20 vol.%). Samples were pressed at 530 MPa and 120 °C for 30 min. These experimental parameters are based on a prior report by Kang et al. that determined the optimized conditions for ZnO densification [12]. This set of samples was pressed in the pellet die heated by the 400 W band heater, which caused the slightly slower ramp rate as compared to the remainder of the experiments presented in this paper. Based on prior experience, the authors do not expect this difference in ramp rate to significantly impact final densities of these samples using aqueous solutions, and it does not change the conclusions drawn from this experiment. This data set is primarily shown to provide context for the present work using non-aqueous transport phases.

The resulting densities and sintegrams for the samples cold-sintered with $Zn(OAc)_2$ aqueous solutions are shown in Fig. 1a, b, respectively, with SEM images shown in Fig. 2. Sintegrams in Fig. 1b are represented as percent compaction, where each compaction trace is normalized and then scaled according to its final density. This method accounts for minute differences in the initial compaction events (*e.g.*, before compaction is recorded) that cause variations in the total compaction amount for samples of identical density. Later sintegrams are also represented this way for consistency.

Figure 1b shows that pellets sintered using 0.8–1.2 M solutions appear to plateau in compaction around 25–30 min, indicating maximum density is achieved. Figure 1a confirms these interpretations where these three samples reach ~ 97% relative density. However, samples sintered with solutions less than 0.8 M do not reach full density in 30 min, achieving densities of 85%, 90%, and 95% for 0.2 M, 0.4 M, and 0.6 M, respectively. SEM images support this result (Fig. 2), showing decreasing porosity (indicating increasing density) with increasing

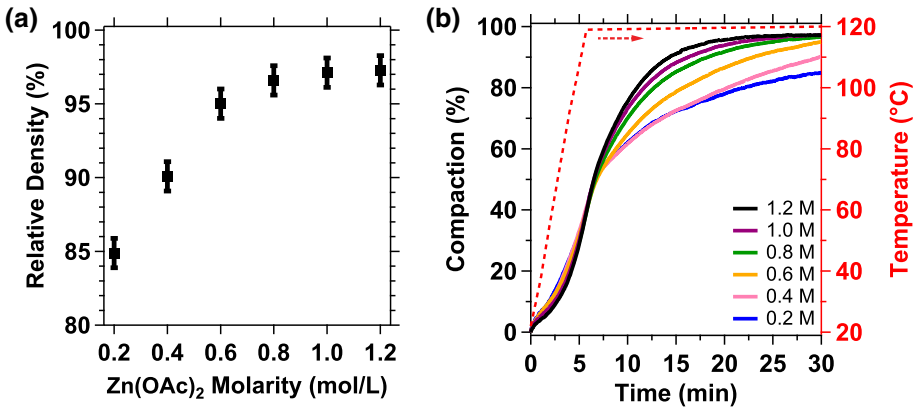

Figure 1 **a** Relative density vs. $Zn(OAc)_2$ solution molarity for samples pressed for 30 min at 530 MPa and 120 °C using 4 wt.% $Zn(OAc)_2$ solution. **b** Sintegrams of ZnO plus 4 wt.% $Zn(OAc)_2$ aqueous solution pressed for 30 min at 530 MPa and 120 °C. Compaction is scaled with respect to final density of the sample. Temperature is shown as the dashed red line with arrow pointing at the associated red axis.

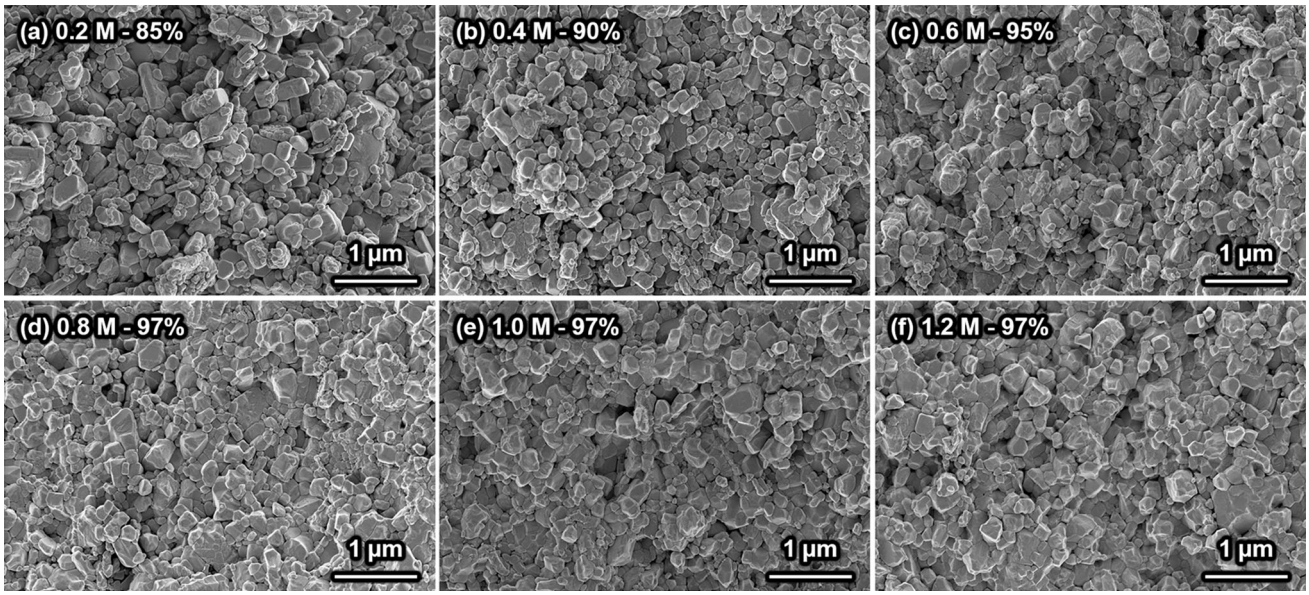

Figure 2 SEM images of cold-sintered ZnO samples using 4 wt.% **a** 0.2 M, **b** 0.4 M, **c** 0.6 M, **d** 0.8 M, **e** 1.0 M, **f** 1.2 M $Zn(OAc)_2$ aqueous solution, pressed at 530 MPa and 120 °C for 30 min. Relative density is shown at the end of each label.

solution molarity. In addition, as solution concentrations increase above 0.8 M, grains appear to become more faceted.

Interestingly, the sintegrams in Fig. 1b show a continuing compaction trend at 30 min for low molarity solutions. This type of information was previously unobtainable as discussed in previous work [17]. A second series of experiments was completed using the same conditions as before, except allowed samples to compact at temperature for 6 h instead of 30 min. Figure 3a, b shows the relative density vs. $Zn(OAc)_2$ solution molarity and resulting sintegrams, respectively, and Fig. 4 shows SEM images of 0.2–1.2 M samples.

Figure 3a shows samples cold-sintered with solutions 0.4 M or higher reached near-full density (> 97%) after 6 h of compaction. The sintegram in Fig. 3b further shows that complete compaction was not reached by the 0.2 M case after 6 h, although relative density increased from 85 to 94% between 30 min and 6 h. It is likely that continuing the experiment for longer time periods would allow for full densification. This result also draws into question the required concentration of transport phase

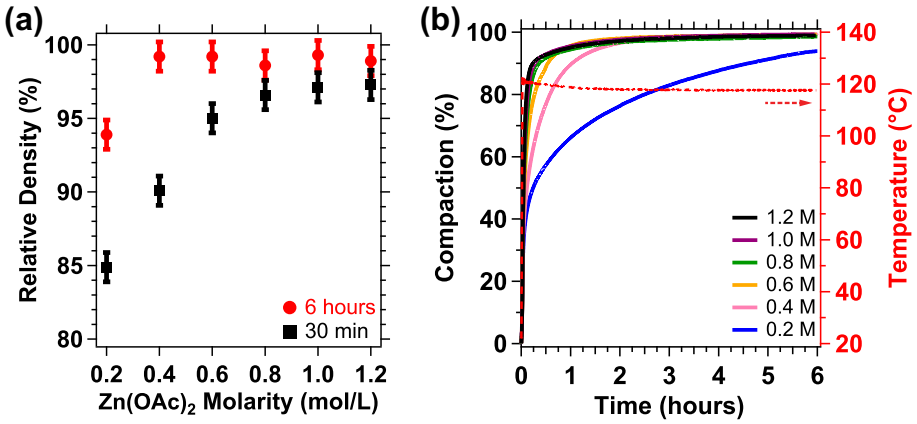

Figure 3 **a** Relative density vs. $Zn(OAc)_2$ solution molarity for samples pressed for 30 min (black squares) and 6 h (red circles) at 530 MPa and 120 °C using 4 wt.% $Zn(OAc)_2$ solution. **b** Sintegrams of ZnO plus 4 wt.% $Zn(OAc)_2$ aqueous solution pressed for 6 h at 530 MPa and 120 °C. Note the change in time scale compared to Fig. 1b.

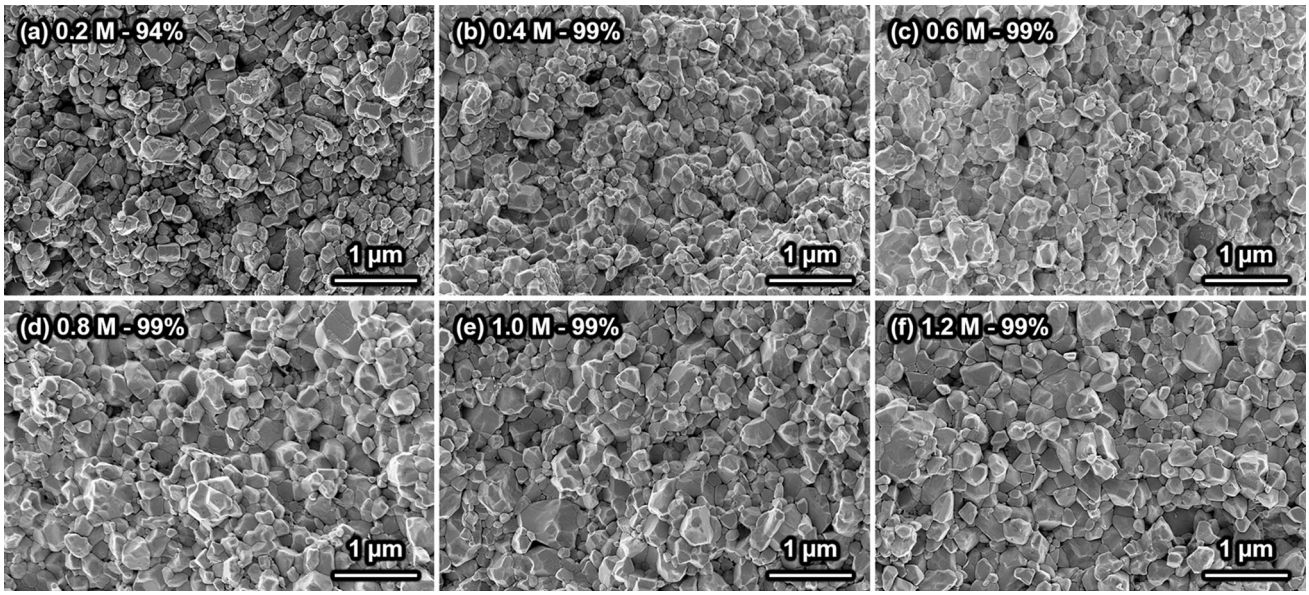

Figure 4 SEM images of cold-sintered ZnO samples using 4 wt.% (a) 0.2 M, (b) 0.4 M, (c) 0.6 M, (d) 0.8 M, (e) 1.0 M, (f) 1.2 M $Zn(OAc)_2$ aqueous solution, pressed at 530 MPa and 120 °C for 6 h.

necessary to achieve full density. A prior report determined the necessary conditions for densification of ZnO using a 0.8 M $Zn(OAc)_2$ solution and found that a 30-min process time was sufficient for densification [12]. The above results confirm this finding, but also highlight that additional process time can compensate for reduced quantity of transport species. This information is important considering the comparison of cold sintering with liquid-phase sintering, where final material properties and behavior can be altered based on secondary phases leftover from the added transport phase [20–23].

TGA was conducted to investigate residual secondary phase content in these cold-sintered ZnO samples and is shown in Fig. 5. Sample (a) is starting ZnO powder, (b) is ZnO powder mixed with 4 wt.% 0.4 M $Zn(OAc)_2$ aqueous solution (prior to cold sintering), (c) and (d) are identically prepared samples (ZnO with 4 wt.% 0.4 M $Zn(OAc)_2$ aqueous solution) pressed at 120 °C for 30 min and 6 h, respectively, that were crushed into coarse powder following cold sintering and put in the TGA.

As shown in trace (a), when heated to 200 °C the ZnO starting powder only shows a mass loss of ~ 0.1%, likely related to adsorbed water. TGA reveals a

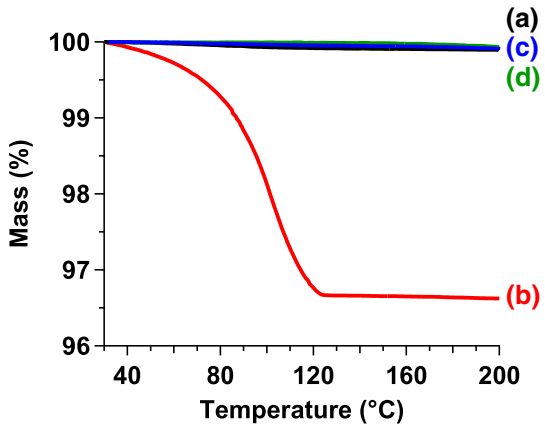

Figure 5 TGA traces of (**a**) ZnO powder, (**b**) ZnO powder mixed with 4 wt.% of 0.4 M $Zn(OAc)_2$ solution, (**c**) ZnO plus 4 wt.% of 0.4 M $Zn(OAc)_2$ solution cold-sintered at 120 °C for 30 min, and (**d**) ZnO plus 4 wt.% of 0.4 M $Zn(OAc)_2$ solution cold-sintered at 120 °C for 6 h.

mass loss of ~ 3.5% in the freshly mixed powder (b), which is comparable to the amount of added transport phase (4 wt.%). This loss is attributed to the evaporation of the aqueous phase. For trace (c), ZnO cold-sintered for 30 min (relative density of 90%), mass loss is roughly the same as the starting powder (< 0.1%) and negligible when compared to that of the mixed powder pre-cold sintering. For sample (d), ZnO cold-sintered for 6 h (relative density > 97%), mass loss is also negligible. No conclusive differences between traces (a), (c), and (d) can be determined with the current instrument setup. Given that nearly all of the liquid water added via the aqueous transport phase appears to have left the system within the first 30 min of cold sintering, it can be inferred that much of the mass transport during this process occurs through a mechanism related to chemisorbed and physisorbed water. This finding motivated further investigations on the role of water in the cold sintering process.

Densification using crystalline $Zn(OAc)_2{\cdot}2H_2O$

The observations above prompted the following set of experiments using $Zn(OAc)_2{\cdot}2H_2O$ powder, without additional liquid water, as the transport phase. For consistency, sintering experiments using a solid $Zn(OAc)_2{\cdot}2H_2O$ transport phase were formulated such that the molar ratio of zinc atoms in the transport phase (Zn*) to ZnO powder (Zn) mimicked the ratio for sintering experiments with aqueous solutions. Table 2 shows comparisons between aqueous solution molarity, transport phase to oxide powder Zn ratios, and added transport phase in weight percent.

Effects of humidity on densification

Given the propensity for powder compacts to interact with atmospheric water, particularly in the presence of water-sensitive acetate salts, an initial experimental set exploring the effects of relative humidity on ZnO densification was necessary. Samples containing 0.95 wt.% $Zn(OAc)_2{\cdot}2H_2O$ were equilibrated in an 85% relative humidity chamber for one day to achieve water saturation, then subsequently divided into individual chambers with fixed relative humidities using the saturated salt solutions listed in Table 1 for two days. Samples were quickly loaded into pellet dies and sintered at 530 MPa and 120 °C for 1 h. Figure 6a, b shows relative density vs. relative humidity and corresponding sintegrams, respectively. SEM images are shown in Fig. 7.

As depicted by Figs. 6a and 7, dense ZnO can be obtained by cold sintering with a crystalline $Zn(OAc)_2{\cdot}2H_2O$ transport phase containing only structural water and small quantities of adsorbed/absorbed water. Figure 6a shows that final density increases from 86 to 96% when samples were stored in 24% and 54% relative humidity environments, respectively. This result indicates a minimum amount of water must be adsorbed to the surface of the ZnO grains or absorbed by the acetate, in addition to the structurally bound water from the acetate, for densification to occur. Although not shown, these results coincide with previous observations related to seasonal humidity changes. Powders prepared in ambient laboratory conditions at relative humidities above 50% (summer) densify above 95%, while powders prepared below 50% relative humidity (winter), regardless of the amount of added transport phase, were limited to densities of 90%. SEM images in Fig. 7 support the results in Fig. 6 and show increasing density with increasing relative humidity, as well as increased faceting in samples that achieved full density.

Measuring mass gain of the powders following storage in the humidity chambers revealed that the powders gained a few milligrams of mass at most (approximately tenths of weight percent). These mass

Table 2 Molarity of aqueous solution converted to ratio of added transport species (Zn*) to parent oxide species (Zn), and to wt.% of added $Zn(OAc)_2{\cdot}2H_2O$

Aqueous solution molarity	Zn*:Zn	Wt.% of $Zn(OAc)_2{\cdot}2H_2O$
0.2	0.6×10^{-3}	0.17
0.6	1.9×10^{-3}	0.50
0.8	2.4×10^{-3}	0.65
1.0	3.0×10^{-3}	0.80
1.2	3.5×10^{-3}	0.95
N/A	5.7×10^{-3}	1.54

For aqueous solutions, 4 wt.% of solution was used

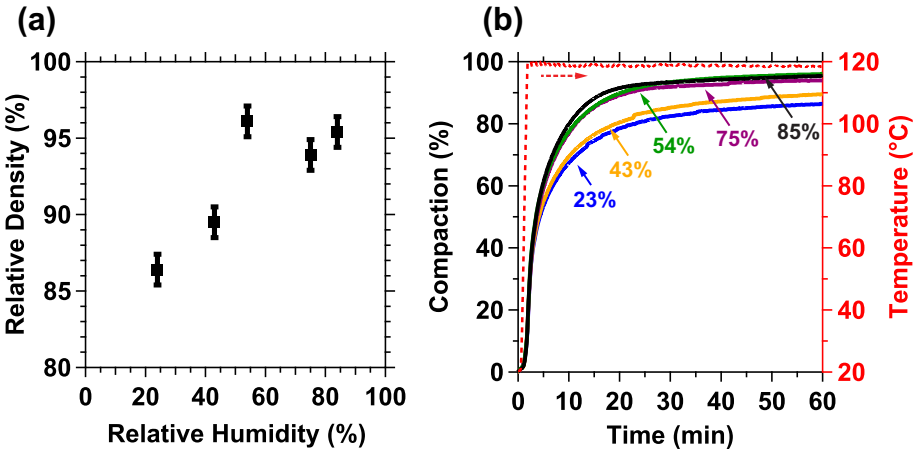

Figure 6 **a** Relative density vs. relative humidity (at 20 °C) of ZnO samples with 0.95 wt.% $Zn(OAc)_2{\cdot}2H_2O$ powder equilibrated for two days at the corresponding relative humidity then cold-sintered at 530 MPa and 120 °C for 1 h and **b** sintegrams of cold-sintered samples with corresponding relative humidity shown for each trace. Temperature in **b** is shown by the dashed red line.

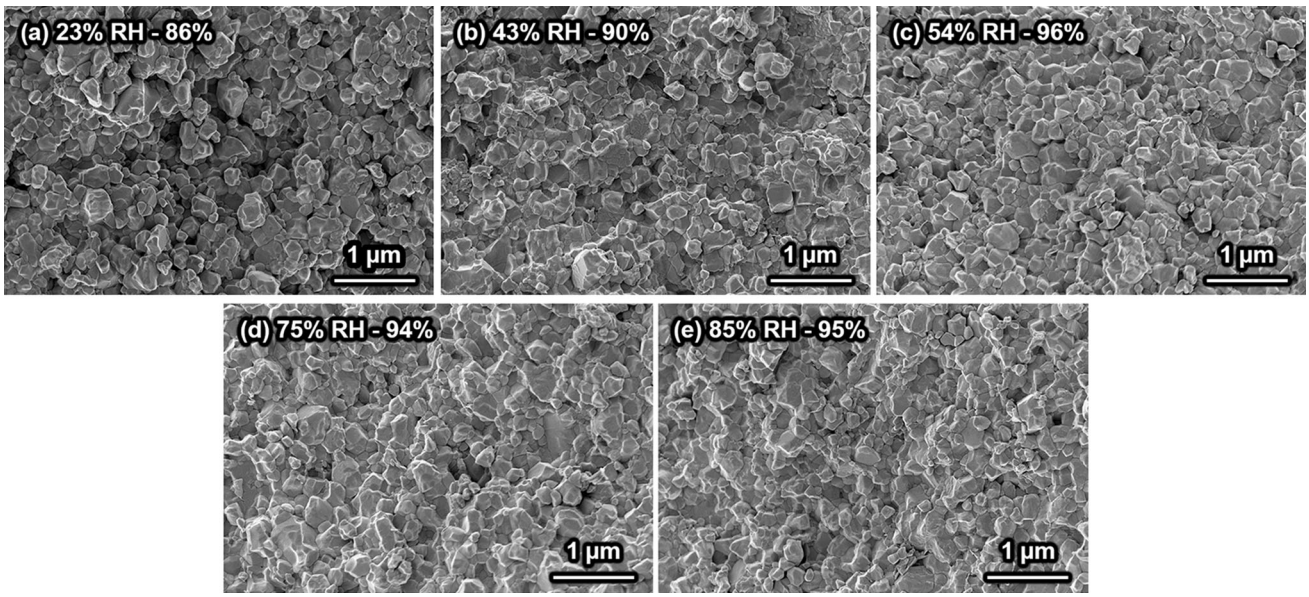

Figure 7 SEM images of ZnO samples with 0.95 wt.% $Zn(OAc)_2{\cdot}2H_2O$ powder equilibrated for two days at **a** 23%, **b** 43%, **c** 54%, **d** 75%, and **e** 85% relative humidity then cold-sintered at 530 MPa and 120 °C for one hour.

gains are at the resolution of the laboratory scale used; therefore, it is difficult to directly correlate density with the amount of water adsorbed or absorbed by the powders. However, these results do indicate that the critical water value is on the order of monolayers of water. This indicates that densification using crystalline $Zn(OAc)_2{\cdot}2H_2O$ likely is not dominated by a dissolution–precipitation mechanism, as previously used to describe cold sintering with aqueous solutions [12, 13], given that such small quantities of water could not sustain significant dissolution. Rather, the densification mechanism may be more closely related to a water-enhanced diffusion process, as proposed by a few others [24, 25]. Dargatz et al. and Gonzalez-Julian et al. reported that small quantities (~ 1.5 wt.%) of adsorbed water could greatly enhance ZnO densification during SPS and allow for sintering at lower temperatures by changing diffusion pathways and defect chemistry [25, 26]. Additionally, Sengul et al. discuss how adsorbed water may promote hydroxylation of the zinc oxide particle surface, thereby increasing surface diffusion and ion adsorption [24]. Equilibrating the powders in a humid environment may also lead to liquid formation near the particle–particle contacts due to capillary condensation [27].

Figure 8 presents x-ray diffraction traces comparing ZnO starting powder to ZnO samples cold-sintered with an aqueous $Zn(OAc)_2$ transport phase and a crystalline $Zn(OAc)_2{\cdot}2H_2O$ transport phase. It can be seen that all peaks in both samples are attributed to the wurtzite phase of ZnO and no secondary phases are detected via XRD in the cold-sintered samples. It is expected that some residual zinc acetate remains in the cold-sintered samples, given that the decomposition temperature of $Zn(OAc)_2$ is well above 120 °C [28–30]; however, residual acetate is likely not detected by XRD because the small quantities used (< 1 wt.%) or because the remaining acetate is no longer crystalline. Alternative characterization techniques better suited for detecting small quantities of acetate, such as Raman spectroscopy, will be used in future studies to further analyze any secondary phases in the cold-sintered samples.

Effects of transport phase concentration on densification

A second series of experiments varied the ratio of $Zn(OAc)_2{\cdot}2H_2O$ to ZnO at a constant humidity. Samples were mixed using the ratios in Table 2 and stored in an 85% relative humidity chamber for two days. Cold sintering conditions were identical to the previous experiment (530 MPa, 120 °C, 1 h). Figure 9a, b show relative density vs. Zn*:Zn and sintegrams, respectively, while Fig. 10 provides SEM images for each formulation post-sintering.

Compaction behavior of the solid-based experiments shown in Fig. 9b differs both in time and total compaction from the compaction behavior of the liquid-based experiments in Fig. 1b. First, increasing concentration of Zn* leads to increasing density with a sudden onset occurring around 1.9×10^{-3} (Fig. 9a),

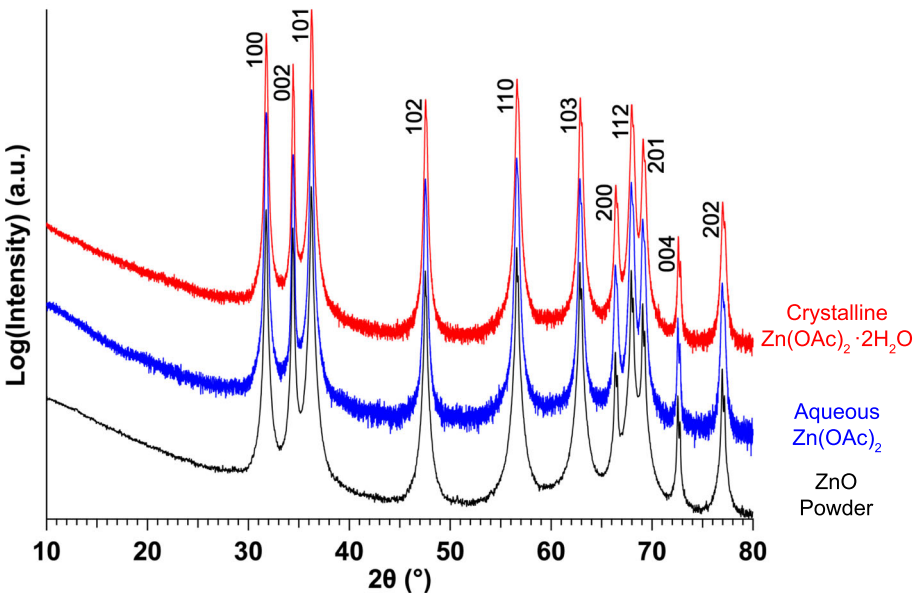

Figure 8 Representative x-ray diffraction patterns of starting ZnO powder (bottom), a ZnO sample cold-sintered with 4 wt.% of a 0.8 M aqueous zinc acetate solution (middle), and a ZnO sample cold-sintered with 0.95 wt.% (Zn*:Zn of 3.5×10^{-3}) of crystalline $Zn(OAc)_2{\cdot}2H_2O$ after equilibrating at 54% RH (top). Samples were cold-sintered at 120 °C under 530 MPa of pressure for 30 min (similar traces were seen for samples cold-sintered for 1 h).

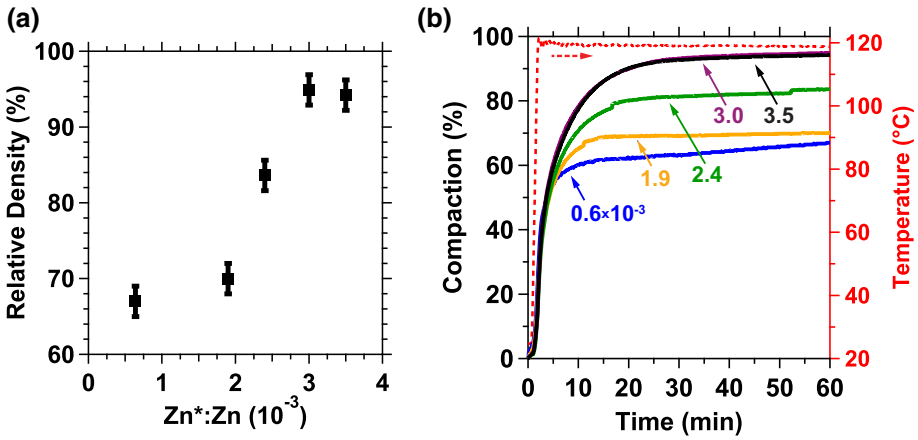

Figure 9 **a** Relative density vs. Zn*:Zn of ZnO samples equilibrated for two days at 85% relative humidity then cold-sintered at 530 MPa and 120 °C for one hour and **b** sintegrams of these samples. Temperature in **b** is shown by the dashed red line and Zn*:Zn ratios are listed below each trace (exponent and base removed for brevity).

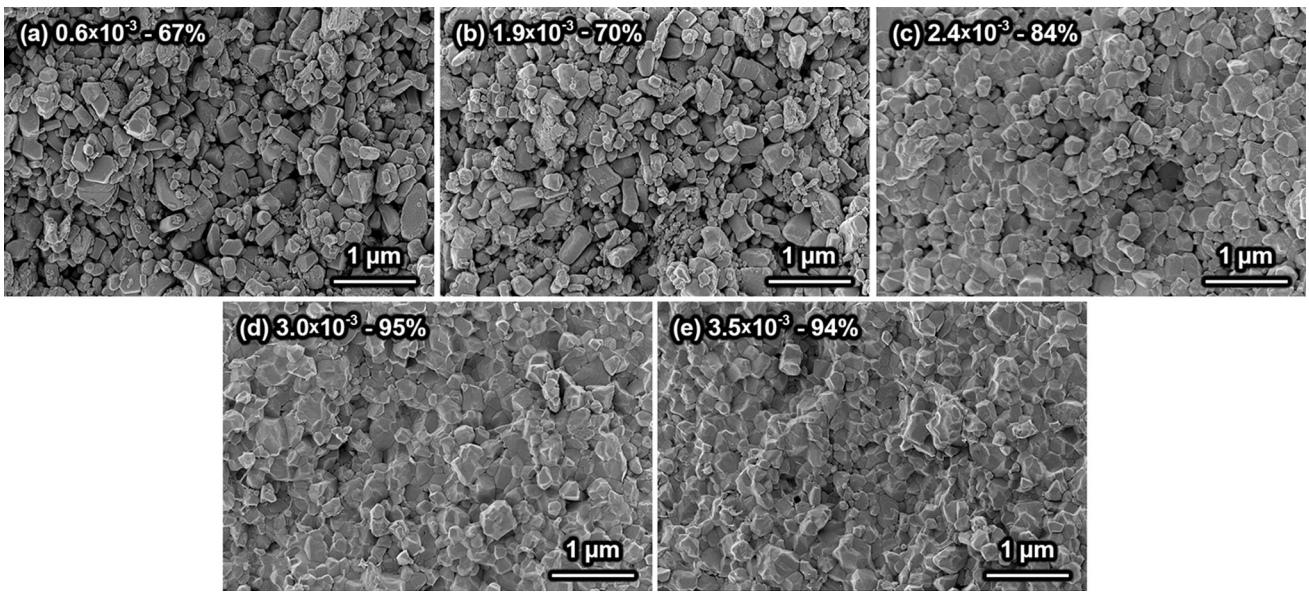

Figure 10 SEM images of ZnO samples with **a** 0.6×10^{-3}, **b** 1.9×10^{-3}, **c** 2.4×10^{-3}, **d** 3.0×10^{-3} and **e** 3.5×10^{-3} Zn*:Zn ratios equilibrated for two days at 85% relative humidity then cold-sintered at 530 MPa and 120 °C for one hour.

implying a critical amount of transport phase is necessary for densification. However, unlike liquid-based experiments, increased process time does not lead to significant changes in compaction (Fig. 9b). This may be related to aqueous and crystalline transport phases leading to different initial compaction rates. It has been previously shown that aqueous transport phases are transient during cold sintering, with the water evaporating or being extruded out of the die over time [12, 13]. The data presented in this manuscript demonstrate that these aqueous-based transport phases frequently contribute an excess of water to the system, which may be slowing compaction at the beginning of the process when there are large quantities of water between the powder particles. As time progresses and water leaves the system, particles continue to compact further. However, when using crystalline transport phases and only small quantities of adsorbed or structural water, this water-mediated compaction does not occur, and compaction occurs much faster initially. Figure 11 shows the derivative of smoothed compaction traces from Fig. 9b to better visualize the change in compaction with time.

Plots of derivatives show (1) increasing ratio of Zn*:Zn results in more rapid compaction, (2) increasing Zn*:Zn beyond 3.0×10^{-3} does not change the compaction rate, and (3) peak compaction rate occurs at the maximum process temperature for all experiments. While the first result follows previous

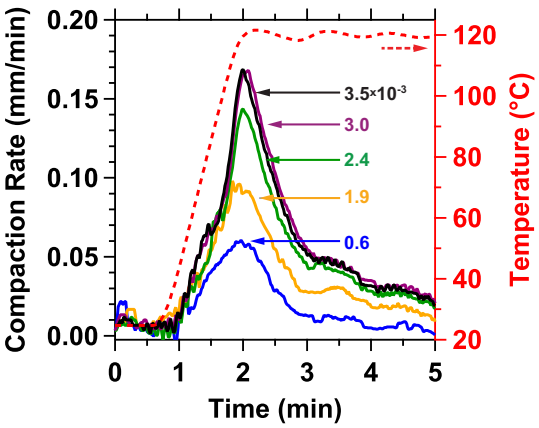

Figure 11 Derivative of smoothed, thermally-corrected compaction data from Fig. 9b. Trace labels correspond to Zn*:Zn ratio with exponent and base removed for brevity. The smoothing routine used a 9-point moving average. Ringing in smoothed data is related to the temperature controller PID settings [17].

observations, the second and third do not and imply transport is limited by the 120 °C process temperature. These last two results prompted another experimental set which increased process temperature to 200 °C, with the corresponding plot of compaction rate vs. time shown in Fig. 12.

Samples processed at 200 °C completed compaction within 5 min (i.e., $dC/dt \rightarrow 0$) compared to the samples processed at 120 °C in Fig. 11. Further investigation of the derivate plot in Fig. 12 reveals multiple features not found at lower process temperatures. First, increasing Zn* delays the compaction completion (i.e., $dC/dt \rightarrow 0$), up to 2.4×10^{-3} Zn*:Zn, after which the trend is reversed. While not clearly understood at this time, future experiments will seek to further investigate this finding.

Second, each trace exhibits multiple peaks, emphasized in Fig. 13. Both samples processed at 120 °C and 200 °C exhibit peak 1 at T ~ 80–90 °C, which may be related to dehydration and evaporation of water from the $Zn(OAc)_2{\cdot}2H_2O$ and ZnO surfaces [28, 29]. Although not shown, identically processed ZnO with no added transport phase (i.e., Zn*:Zn = 0) was pressed and also exhibited this peak, further suggesting its association with water loss. Peaks 2 and 3 are only visible in the samples processed at 200 °C and may be attributed to decomposition of the transport phase. This is supported by the observation that the peak compaction rate occurs before the maximum process temperature is reached for samples processed at 200 °C and by the fact that compaction rate quickly falls to zero after peaking, which is not the case for samples processed at 120 °C. Furthermore, the densities of the samples cold-sintered at 200 °C never exceeded 85%, with several of the samples not robust enough to withstand extraction from the die and volumetric density measurements.

Decomposition pathways of $Zn(OAc)_2{\cdot}2H_2O$ are well studied and heavily depend on local atmosphere and heating rate [28–31]. Arii et al. conducted TG–DTA analysis of $Zn(OAc)_2{\cdot}2H_2O$ heated in dry He and saw a dehydration event at 76 °C and possible melting or sublimation, creating basic zinc acetate ($Zn_4O(CH_3CO_2)_6$), at ~ 250 °C [28]. A second

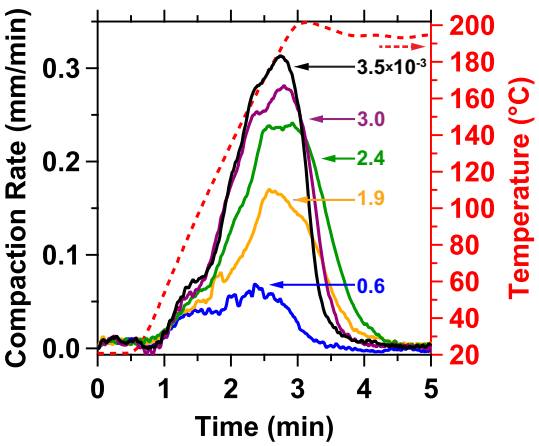

Figure 12 Derivative of compaction traces for ZnO samples equilibrated for two days at 85% relative humidity then cold-sintered at 530 MPa and 200 °C for one hour, with the same smoothing routine as Fig. 11. Trace labels correspond to Zn*:Zn ratio (exponent and base removed for brevity).

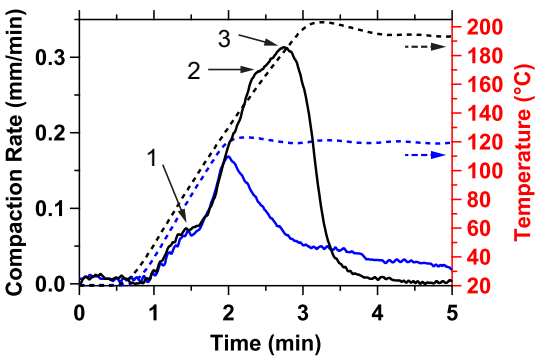

Figure 13 Plot of dC/dt, or compaction rate, (solid lines) and temperature (dashed lines) for 3.5×10^{-3} Zn*:Zn samples processed at 120 °C (blue) and 200 °C (black). The visible peaks are numbered, with only the first peak prominent in the sample processed at 120 °C.

analysis in a controlled humidity environment revealed that increasing the partial pressure of H_2O altered the reaction pathway, promoting the decomposition of anhydrous $Zn(OAc)_2$ into ZnO, rather than decomposition into basic zinc acetate or sublimation of the anhydrous zinc acetate. The TG–DTA data combined with XRD data collected at varying temperatures showed that the decomposition of $Zn(OAc)_2$ to ZnO begins around 180 °C and is completed around 200 °C [28]. Peaks 2 and 3 in Fig. 13 may be related to this decomposition of $Zn(OAc)_2$ to ZnO. These peaks are observed at temperatures slightly lower than expected based on the report from Arii et al. [28]; however, this could be related to the unique cold sintering conditions (i.e., high pressures, fast heating rates, etc.). Although further investigations are needed to probe the effects of atmosphere and pressure on cold sintering reactions, it is interesting to note potential observation of transport phase decay.

Lastly, SEM images (Fig. 14) of the samples processed at 200 °C show a significant change in morphology and grain size after increasing Zn*:Zn above 1.9×10^{-3}, which is not observed at 120 °C. It is likely a combination of temperature and a critical amount of transport phase that promotes grain growth on the order of 150%. This grain growth could again be related to the decomposition of the transport phase. As previously mentioned, the comparatively low densities of the samples cold-sintered at 200 °C indicate limited densification-promoting diffusion. It is possible that the higher temperature (200 °C) and fast heating rate (80 °C/min) cause the transport phase to decompose before it can promote significant mass transport leading to complete densification. Furthermore, the zinc acetate decomposes into ZnO on the particle surfaces [28]. Higher concentrations of added zinc acetate may lead to increased surface diffusion and increased formation of ZnO, contributing to the large grain growth. Funahashi et al. saw similar grain growth as they increased the concentration of the added acetic acid transport phase when cold sintering ZnO at 238 °C [32]. However, the sample with large grain growth still achieved a high density (98%), which could be related to the higher decomposition temperature of acetic acid (> 400 °C) and the much slower ramp rate (5 °C/min). While the above explanation for the observed grain growth has not been confirmed and this phenomenon is not fully understood at present, the sintegrams have undoubtedly provided an additional level of information that would otherwise not be acquired. With additional experimentation, potential correlations between cold sintering mechanisms and processes studied by other characterization methods may be found.

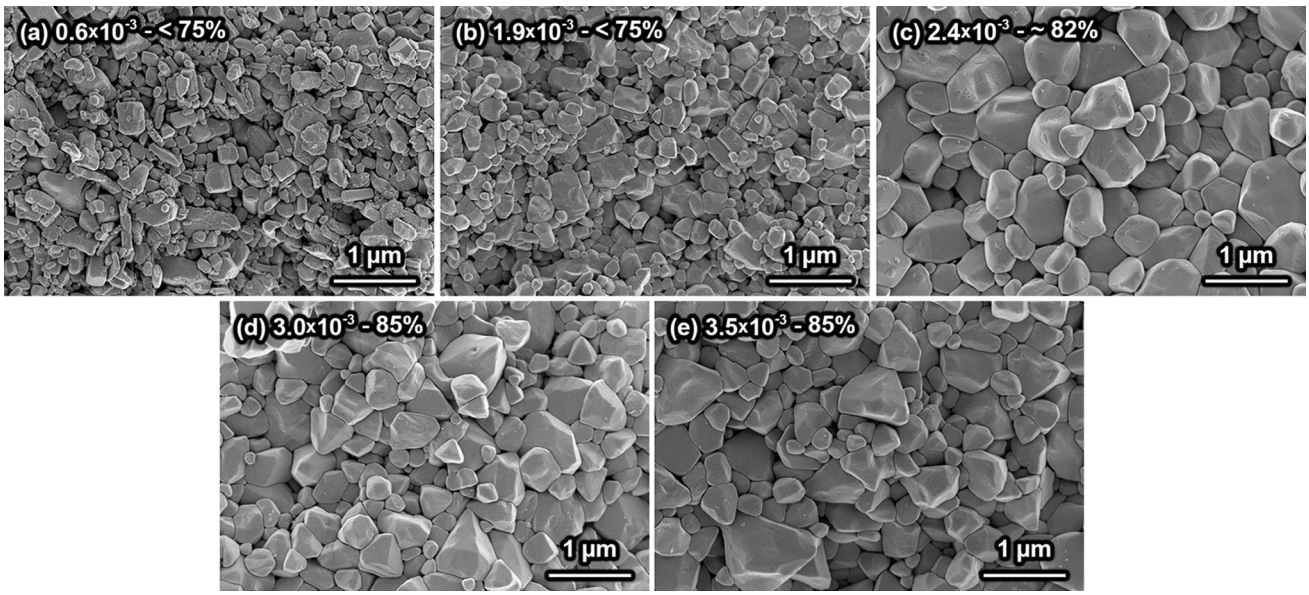

Figure 14 SEM images of ZnO samples with **a** 0.6×10^{-3}, **b** 1.9×10^{-3}, **c** 2.4×10^{-3}, **d** 3.0×10^{-3} and **e** 3.5×10^{-3} Zn*:Zn ratios cold-sintered at 530 MPa and 200 °C for one hour. Densities are included on the micrographs; however, several samples broke or chipped due to their low densities, so accurate measurements were difficult to obtain.

Conclusions

Long-term (6 h) cold sintering of ZnO with aqueous-based transport phases was shown. Previous publications showed near 100% densification occurring with 0.8 M zinc acetate aqueous solutions in 30 min process time [12]. Increasing process time allows for equal densification using 0.4 and 0.6 M solutions. However, TGA analysis reveals little mass loss occurring in a sample after 30 min of cold sintering even though density increases from 90 to > 97% if an additional 5.5 h of process time are allowed. This indicates significantly lower quantities of water are necessary to facilitate densification during cold sintering than previously believed. In light of this conclusion, investigation of cold sintering using a crystalline transport phase containing only structural and adsorbed water was conducted. ZnO samples with densities up to 96% were obtained by cold sintering with a crystalline $Zn(OAc)_2{\cdot}2H_2O$ transport phase. This result led to the conclusion that the primary means of mass transport during cold sintering occurs via a mechanism not associated with excess liquid water in the system, but rather the structural and adsorbed water, at least when using crystalline transport phases. Furthermore, compaction appears to occur more quickly at the beginning of the cold sintering process when using crystalline $Zn(OAc)_2{\cdot}2H_2O$, as increased process times did not lead to additional densification. Excess water in aqueous transport phases may initially slow the compaction process until the water begins to leave the system via evaporation or extrusion out of the die.

Humidity greatly affects densification in the ZnO–$Zn(OAc)_2{\cdot}2H_2O$ system, requiring processing conditions above 50% relative humidity to reach near-full density. At constant humidity and process temperatures of 120 °C, density shows a remarkable increase at 2.4×10^{-3} ratio of Zn*:Zn, with microstructure supporting this result. Increasing process temperatures to 200 °C results in lower density samples and two additional peaks in the differential sintegram, which may be related to decomposition and phase changes in the transport phase. Microstructures reveal a large change in morphology and grain size between 2.4 and 3.5×10^{-3} Zn*:Zn for the samples processed at 200 °C, possibly also related to decomposition of the zinc acetate. This finding requires further experimentation to understand the relationship of temperature and transport phase content on grain growth kinetics in a solid-based transport system for cold sintering.

Acknowledgements

The authors would like to acknowledge the use of the Huck Institutes of the Life Sciences' Penn State Microscopy Facility – University Park, PA. This material is based upon work supported by the National Science Foundation, as part of the Center for Dielectrics and Piezoelectrics under Grant Nos. IIP-1841453 and 1841466. This material is based upon work supported by the National Science Foundation Graduate Research Fellowship Program under Grant Nos. DGE-1252376 and DGE-1255832. Any opinions, findings, and conclusions or recommendations expressed in this material are those of the author(s) and do not necessarily reflect the views of the National Science Foundation.

Compliance with ethical standards

Conflicts of interest The authors declare that they have no any conflict of interest.

References

[1] Guo J, Guo H, Baker AL, Lanagan MT, Kupp ER, Messing GL, Randall CA (2016) Cold sintering: a paradigm shift for processing and integration of ceramics. Angew Chemie Int Ed 55:11457–11461

[2] Maria JP, Kang X, Floyd RD, Dickey EC et al (2017) Cold sintering: current status and prospects. J Mater Res 32:3205–3218

[3] Guo J, Floyd R, Lowum S, Maria J-P, Herisson De Beauvoir T, Seo J-H, Randall CA (2019) Cold Sintering: progress, challenges, and future opportunities. Annu Rev Mater Res 49:275–295

[4] Kang X, Floyd R, Lowum S, Long D, Dickey E, Maria JP (2019) Cold sintering with dimethyl sulfoxide solutions for metal oxides. J Mater Sci 54:7438–7446. https://doi.org/10.1007/s10853-019-03410-1

[5] Berbano SS, Guo J, Guo H, Lanagan MT, Randall CA (2017) Cold sintering process of $Li_{1.5}Al_{0.5}Ge_{1.5}(PO_4)_3$ solid electrolyte. J Am Ceram Soc 100:2123–2135

[6] Leng H, Huang J, Nie J, Luo J (2018) Cold sintering and ionic conductivities of $Na_{3.256}Mg_{0.128}Zr_{1.872}Si_2PO_{12}$ solid electrolytes. J Power Sources 391:170–179

[7] Ma JP, Chen XM, Ouyang WQ, Wang J, Li H, Fang JL (2018) Microstructure, dielectric, and energy storage properties of $BaTiO_3$ ceramics prepared via cold sintering. Ceram Int 44:4436–4441

[8] Bin HW, Li L, Cao M, Chen XM (2018) Plastic deformation and effects of water in room-temperature cold sintering of NaCl microwave dielectric ceramics. J Am Ceram Soc 101:4038–4043

[9] Jing Y, Luo N, Wu S, Han K, Wang X, Miao L, Wei Y (2018) Remarkably improved electrical conductivity of ZnO ceramics by cold sintering and post-heat-treatment. Ceram Int 44:20570–20574

[10] Induja IJ, Sebastian MT (2017) Microwave dielectric properties of mineral sillimanite obtained by conventional and cold sintering process. J Eur Ceram Soc 37:2143–2147

[11] Medri V, Servadei F, Bendoni R, Natali Murri A, Vaccari A, Landi E (2019) Nano-to-macroporous TiO_2 (anatase) by cold sintering process. J Eur Ceram Soc 39:2453–2462

[12] Kang X, Floyd R, Lowum S, Cabral M, Dickey E, Maria JP (2019) Mechanism studies of hydrothermal cold sintering of zinc oxide at near room temperature. J Am Ceram Soc 102:4459–4469

[13] Guo H, Baker A, Guo J, Randall CA (2016) Protocol for ultralow-temperature ceramic sintering: an integration of nanotechnology and the cold sintering process. ACS Nano 10:10606–10614

[14] Guo H, Guo J, Baker A, Randall CA (2016) Hydrothermal-assisted cold sintering process: a new guidance for low-temperature ceramic sintering. ACS Appl Mater Interfaces 8:20909–20915

[15] Boston R, Guo J, Funahashi S, Baker AL, Reaney IM, Randall CA (2018) Reactive intermediate phase cold sintering in strontium titanate. RSC Adv 8:20372–20378

[16] Li L, Bin HW, Yang S, Yan H, Chen XM (2019) Effects of water content during cold sintering process of NaCl ceramics. J Alloys Compd 787:352–357

[17] Floyd R, Lowum S, Maria J-P (2019) Instrumentation for automated and quantitative low temperature compaction and sintering. Rev Sci Instrum 90:055104

[18] Greenspan L (1977) Humidity fixed points of binary saturated aqueous solutions. J Res Natl Bur Stand A Phys Chem 81A:89–96

[19] Wexler A, Hasegawa S (1954) Relative humidity-temperature relationships of some saturated salt solutions in the temperature range 0° to 50°C. J Res Natl Bur Stand 53:19–26

[20] Corker DL, Whatmore RW, Ringgaard E, Wolny WW (2000) Liquid-phase sintering of PZT ceramics. J Eur Ceram Soc 20:2039–2045

[21] Fan GF, Shi MB, Lu WZ, Wang YQ, Liang F (2014) Effects of Li_2CO_3 and Sm_2O_3 additives on low-temperature sintering and piezoelectric properties of PZN-PZT ceramics. J Eur Ceram Soc 34:23–28

[22] Chao X, Ma D, Gu R, Yang Z (2010) Effects of CuO addition on the electrical responses of the low-temperature sintered $Pb(Zr_{0.52}Ti_{0.48})O_3$-$Pb(Mg_{1/3}Nb_{2/3})O_3$-$Pb(Zn_{1/3}Nb_{2/3})O_3$ ceramics. J Alloys Compd 491:698–702

[23] Nam C-H, Park H-Y, Seo I-T, Choi J-H, Nahm S, Lee H-G (2011) Effect of CuO on the sintering temperature and piezoelectric properties of MnO2-doped $0.75Pb(Zr_{0.47}Ti_{0.53})O_3$–$0.25Pb(Zn_{1/3}Nb_{2/3})O_3$ ceramics. J Alloys Compd 509:3686–3689

[24] Sengul MY, Guo J, Randall CA, van Duin ACT (2019) Water-mediated surface diffusion mechanism enables the cold sintering process: a combined computational and experimental study. Angew Chemie 131:12550–12554

[25] Gonzalez-Julian J, Neuhaus K, Bernemann M, Pereira da Silva J, Laptev A, Bram M, Guillon O (2018) Unveiling the mechanisms of cold sintering of ZnO at 250°C by varying applied stress and characterizing grain boundaries by Kelvin Probe Force Microscopy. Acta Mater 144:116–128

[26] Dargatz B, Gonzalez-Julian J, Bram M, Shinoda Y, Wakai F, Guillon O (2016) FAST/SPS sintering of nanocrystalline zinc oxide-Part II: abnormal grain growth, texture and grain anisotropy. J Eur Ceram Soc 36:1221–1232

[27] Soustelle M (2016) Thermodynamics of surfaces and capillary systems. ISTE Ltd., London

[28] Arii T, Kishi A (2003) The effect of humidity on thermal process of zinc acetate. Thermochim Acta 400:175–185

[29] Ghule AV, Ghule K, Chen CY, Chen WY, Tzing SH, Chang H, Ling YC (2004) In situ thermo-TOF-SIMS study of thermal decomposition of zinc acetate dihydrate. J Mass Spectrom 39:1202–1208

[30] Hussien GAM (1991) Characterisation of the thermal genesis course of zinc oxide from zinc acetoacetonate dihydrate. Thermochim Acta 186:187–197

[31] Baraldi P (1982) Thermal behavior of metal carboxylates: III-metal acetates. Spectrochim Acta A Mol Spectrosc 38A:51–55

[32] Funahashi S, Guo J, Guo H, Wang K, Baker AL, Shiratsuyu K, Randall CA (2017) Demonstration of the cold sintering process study for the densification and grain growth of ZnO ceramics. J Am Ceram Soc 100:546–553